Research article

Investigation of the insecticidal potential of curcumin derivatives that target the *Helicoverpa armigera* sterol carrier protein-2

Naeema Kausar [a], Wayne Thomas Shier [b], Mahmood Ahmed [c], Maryam [a], Norah A. Albekairi [d], Abdulrahman Alshammari [d], Muhammad Saleem [e], Muhammad Imran [f,**], Muhammad Muddassar [a,*]

[a] *Department of Biosciences, COMSATS University Islamabad, Park Road, Islamabad, 45550, Pakistan*
[b] *College of Pharmacy, Department of Medicinal Chemistry, University of Minnesota, 55455, USA*
[c] *Department of Chemistry, Division of Science and Technology, University of Education, College Road, Lahore, Pakistan*
[d] *Department of Pharmacology and Toxicology, College of Pharmacy, King Saud University, Riyadh, 11451, Saudi Arabia*
[e] *School of Biological Sciences, University of the Punjab, Lahore, Pakistan*
[f] *KAM-School of Life Sciences, FC College (A Chartered University), Lahore, 54000, Pakistan*

A B S T R A C T

Cotton bollworm (*Helicoverpa armigera*) is a highly polyphagous, widely prevalent, and persistent Old World insect pest that affects numerous important crops that are directly consumed by people, including tomato, cotton, pigeon pea, chickpea, rice, sorghum, and cowpea. Insects do not synthesize steroids but obtain them from their diet. Inhibition of dietary uptake of steroids by insects is a potentially effective insecticidal mechanism that should not be toxic to humans and other mammals, who synthesize their steroids. Ten curcumin derivatives were tested against *H. armigera* sterol carrier protein-2 (HaSCP-2) for their potential as insecticidal agents. Curcumin derivatives were initially docked at the binding site of HaSCP-2 to determine their binding affinities and plausible binding modes. The binding modes predominantly show hydrophobic interactions of derivatives with Phe53, Phe110, and Phe89 as core interacting residues in the active site. Validation of *in silico* results was carried out by performing a fluorescence binding and displacement assay to determine the binding affinities of curcumin derivatives. Among a collection of curcumin derivatives tested, Cur10 showed the lowest IC_{50} value of 9.64 μM, while Cur07 was 19.86 μM, and Cur06 was 20.79 μM. There was a significant negative correlation between the ability of the curcumin derivatives tested to displace the fluorescent probe from the sterol binding site of HaSCP-2 and to inhibit *Sf*9 insect cell growth in culture, which is consistent with the curcumin derivatives acting by the novel mechanism of blocking sterol uptake. Then molecular dynamics simulation studies validated the predicted binding modes and the interactions of curcumin derivatives with HaSCP-2 protein. In conclusion, these studies support the potential use of curcumin derivatives as insecticidal agents.

---

* Corresponding author.
** Corresponding author.
E-mail addresses: muhammadimran@fccollege.edu.pk (M. Imran), mmuddassar@comsats.edu.pk (M. Muddassar).

1. Introduction

Cotton bollworm (*Helicoverpa armigera*) is a highly polyphagous, widely prevalent, and persistent Old World insect pest that affects numerous important crops directly consumed by people, including tomato, cotton, pigeon pea, chickpea, rice, sorghum, and cowpea. It has become resistant to currently available control methods, including chemical insecticides [1,2], integrated pest management [3], and genetically modified crops [4,5]. This situation has led scientists to seek alternate, preferably natural approaches to control insect pests. Insects lack key enzymes needed to synthesize sterols for normal growth and development [6], and therefore they depend on dietary sources of sterol precursors such as beta-sitosterol from plants or cholesterol from animals. Because sterols are highly hydrophobic, their absorption from the diet require some carrier like sterol carrier protein-2 (SCP-2) to achieve intestinal absorption of steroids [7]. Blocking the activity of this carrier protein is a particularly attractive mechanism for potential insecticides because effective inhibitors should inhibit insect growth and function by depriving them of an essential nutrient while being non-toxic to humans and other animals who can and do synthesize all the steroids they need and sometimes more.

In this study, we have carried out the initial phases of the evaluation of natural curcumin derivatives as a potential insecticide against *H. armigera,* by inhibition of its sterol carrier protein-2 (HaSCP-2). Curcumins are particularly attractive potential insecticides for use in South Asia because they are natural, relatively hydrophobic molecules that would be expected to interact with HaSCP-2. They are expected to be well-tolerated by the population there, who widely use them as turmeric in local cuisines. Further, studies have shown that dietary curcumins provide health benefits. In a meta-analysis of 14 studies, Yuan et al. [8] reported that the use of turmeric and curcuminoids resulted in reductions in triglycerides (-19.1 mg/dL, $P = 0.003$), total cholesterol (-11.4 mg/dL, $P < 0.0001$), LDL-Cholesterol (-9.83 mg/dL, $P = 0.002$), and HDL-Cholesterol (-1.9 mg/dL, $P = .02$). In humans, dietary curcumins are presumed to be absorbed in a fat-soluble form by an intestinal lymphatic transport mechanism [9], so that inhibition of sterol carrier protein-2 would not be expected to interfere with their health benefits. Furthermore, curcumins have relatively simple structures amenable to chemical synthesis, to synthesize a substantial range of natural derivatives. Curcumins have been used as a potent larvicidal agent to control *Aedes aegypti* [10,11] and to stop the growth of *Gasterophilus intestinalis*, a parasite in the stomach of horses [12]. Other natural compounds like flavonoids [13] have also been used as a pesticide to retard larval growth among different insects like aphids [14]. Another natural product, α-mangostin [15], a xanthonoid isolated from the mangosteen tree (*Garcinia mangostana*), has also been identified as a potential insecticide against mosquitoes [15–17] and *H. armigera* [1,18] by inhibition of SCP-2.

In this study, *in silico,* and *in vitro* methods were adopted to evaluate derivatives of curcumin for their insecticidal potential through inhibition of cholesterol binding to target protein HaSCP-2 by performing molecular docking, molecular dynamic simulations, and fluorescence binding and displacement assays. In addition, *in vitro* toxicity was evaluated in the *Sf*9 *Spodoptera frugiperda* insect cell line by measuring cell growth inhibition rate.

Virtually screened inhibitors of SCP-2 (SCPIs) have been reported and have been tested against mosquitoes [16,18–20]. Botanical preparations including neem, essential oils, and garlic have also been gathered attention to be used as an insect repellent and to ward off insect pests [21]. Keeping this in view scientist has focused on synthesizing derivatives from natural compounds and determining their biological activities like antimicrobial, antifungal, and insecticidal, curcumin which has all these activities and can prove to be an inhibitor molecule to control an infestation of *H. armigera*, a destructive pest of crops.

2. Methods and materials

8-Anilino-1-naphthalene sulfonic acid ammonium salt (1,8-ANS), a chemical probe, and fetal bovine serum (FBS) were purchased from Sigma-Aldrich (St. Louis, MO, USA). MTT (3-(4,5-dimethylthiazol-2-yl)-2,5-diphenyltetrazolium bromide) was purchased from Thermo Fisher Scientific Chemicals (Ward Hill, MA, USA). Grace's Insect Medium was purchased from Gibco (Grand Island, NY, USA). The *Spodoptera frugiperda* insect cell line, *Sf*9, was purchased from Novagen, Millipore Sigma (St. Louis, MO, USA). The software and tools that were used with in-house derivatives of curcumin [22] were Schrodinger Suit 2018-4, AMBER Tools 2021, VMD, and NAMD v. 2.14.

2.1. Retrieval of HaSCP-2 structure

The three-dimensional (3D) NMR structure (PDB ID: 4UEI) of HaSCP-2 was retrieved from the Protein Data Bank (PDB) [1]. The 3D structure of HaSCP-2 was visualized in PyMOL software. The structure contains twenty different conformations, from which the least RMSD value conformation, in comparison with the *Aedes aegypti* crystal structure, AeSCP-2 (PDB ID: 1PZ4) was selected to perform further computational studies.
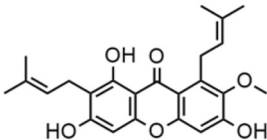
2.2. Molecular docking

Schrodinger (Maestro 2018-4) was used to carry out molecular docking studies. An in-house library of curcumin derivatives [22] (Table 1) was docked with the target protein HaSCP-2 to evaluate their binding affinities and binding mode interactions. GLIDE tool was used to predict the derivative's binding poses and their binding affinities. Molecular docking studies involved an initial protein preparation step, in which hydrogen atoms were added. The protonation properties of the proteins were assigned at physiological pH 7.4 using the PROPKA module in the protein preparation wizard (Maestro). For minimization, OPLS 2005 was applied, and atoms of the systems were submitted in restrained molecular mechanics (MM). Lig-prep wizard (Schrodinger Suit) was used to generate different poses for curcumin derivatives. Structure preparation includes the minimization of structures by applying OPLS 2005 Force

Table 1
Curcumin derivatives are, including their molecular structure, molecular weight, LogP value, and gscore.

Derivative ID	Structure	MW (g/mol)	LogP	gscore (kcal/mol)
Cur01		408.5	4.2	−6.6
Cur02		365.4	3.9	−7.1
Cur03		469.5	4.4	−8.1
Cur04		364.4	3.9	−7.3
Cur05		392.4	3.2	−7.8
Cur06		440.5	6.1	−8.0
Cur07		391.4	3.3	−8.3
Cur08		458.5	4.6	−8.4
Cur09		407.4	2.5	−7.5
Cur10		530.5	4.9	−8.8

Table 1 (*continued*)

Derivative ID	Structure	MW (g/mol)	LogP	gscore (kcal/mol)
Alpha-mangostin (Control)		410.5	4.7	−6.5

Field. Moreover, the addition of hydrogen was carried out for optimization of curcumin derivatives structures, and stereoisomers were generated for each structure, after which they were exported for molecular docking studies. A grid map around HaSCP-2 was generated by specifying the reported binding pocket residues [1] to which curcumin derivatives possibly could bind. Standard precision (SP), and flexible docking were performed. The grid file was imported into Maestro v.11 workspaces along with prepared curcumin derivatives. Five poses for each docked complex were generated. The docked file was analyzed and checked for breakdown of binding affinities and binding mode interactions. Furthermore, the detailed binding interactions of curcumin derivatives with HaSCP-2 were modeled and predicted by BIOVIA-Discovery Studio 2021.

2.3. Fluorescence binding and displacement assay of curcumin derivatives with HaSCP-2

Synthetic curcumin derivatives [22] and the positive control α-mangostin [1,18] were evaluated for their ability to inhibit the binding of cholesterol by HaSCP-2 using a fluorescence binding and displacement assay. It has been reported that physiological ligands of target protein HaSCP-2 e.g., cholesterol and beta-sitosterol can compete for the binding of the fluorescent probe 1,8-ANS to HaSCP-2 [23]. Recombinant HaSCP-2 protein was expressed and purified (unpublished data), and the concentration was measured on the Nanodrop-1000 instrument (Thermo Scientific). The HaSCP-2 protein solution was diluted into 15 μM in 1,8-ANS probe (15 μM) in a reaction buffer (25 mM Na_3PO_4, 75 mM NaCl, 0.1 mM EDTA; pH 7.0) and incubated at 25 °C for 2.5min to allow probe binding. Curcumin derivatives and the control alpha-mangostin in serial working concentrations (2.5–160 μM) were added to the HaSCP-2 + ANS complex and the mixture was allowed to incubate an additional 2.5 min at 25 °C before measuring fluorescence intensity. Fluorescence intensity was measured in triplicate using a Varioskan LUX 3020–80235 microplate reader (Thermo Scientific) controlled by Skanlt Software. Excitation was measured at 360 nm and emission at 480 nm. Background fluorescence values were obtained by incubating the ANS probe with serial working concentrations of derivative only, and the measured fluorescence intensity was subtracted from the fluorescence intensity in the presence of HaSCP-2. 50 % inhibitor concentration (IC_{50}) values were calculated using a single-site competition, nonlinear regression model in GraphPad Prism V.9.4. using the equation:

$$Y = \text{Best fit value MIN} + (\text{best-fit value MAX} - \text{best-fit value MIN}) / (1 + 10^{X-\log EC50})$$

2.4. In vitro toxicity of curcumins in Sf9 (Spodoptera frugiperda) cells

In vitro toxicity measurements for curcumin derivatives and the positive control alpha-mangostin were obtained using the *Sf*9 insect cell line [24–26]. Working dilutions (0.5, 1, 2.5, 5, 10, 25, 50, and 100 μM) of all test samples were made from stock solutions dissolved in DMSO and diluted into Grace's insect medium with 10 % FBS. All working dilutions were made in 100 μL of Grace's medium per well in triplicate in 96-well trays. DMSO was used as a negative control. Wells were inoculated by the addition of a suspension of 2×10^4 *Sf*9 cells/mL in 100 μL of Grace's medium using cells from production flasks counted on a hemocytometer. The trays were incubated at 30 °C in a humidified, non-CO_2 incubator for at least 3–5 days examining the wells daily under the microscope until the cultures reached near confluency in the control wells. Growth of viable *Sf*9 insect cells was estimated by adding 100 μL of MTT (3-(4,5-dimethylthiazol-2-yl)-2,5-diphenyltetrazolium bromide) (5 mg/mL) in saline and incubating for 4 h at 30 °C. Viable cell number was scored by formazan formation visually or by adding 100 μL of DMSO to wells and measuring absorbance at 570 nm on a Spectra Max (Molecular Devices). The relative inhibition of growth rate (IR) for cells treated with curcumin derivatives was calculated by the equation [27] (1−At/Ac) x 100 = IR, in which At = absorbance value of tested wells and Ac = absorbance value of control wells. Data were represented as mean ± SD.

2.5. Molecular dynamic simulations (MD)

The selected curcumin complexes as well as the positive control, alpha-mangostin, were subjected to 100 ns simulation to explore the complex stability by using VMD [28] and NAMD [29] tools. The LeaP [30] program of AMBER21 tools [31] was used to add the missing hydrogens to the HaSCP-2 protein and antechamber was used to assign the partial charges to ligands by utilizing the AM1-BCC model. All the complexes were solvated in an orthorhombic box of size 10 Å containing TIP3P water molecules [32]. The solvated systems were then neutralized by adding Na^+ and Cl^- counter ions. AMBER forcefields, ff14SB [33], and GAFF [34] were used to parametrize the protein and ligands respectively. To avoid steric clashes, all the systems were minimized using 10000 steps, before simulation. All the atoms of the protein were fixed before equilibrating the water molecules. To stabilize the systems, additional

equilibrations were performed at the following three different temperatures: 200 K, 250 K, and 300 K for 10 ps. Ultimately, all the systems were employed for 100 ns simulation by using an NPT ensemble with 310 K temperature and 1 atm pressure. All the bonds were constrained by using the SHAKE [35] algorithm while the Particle Mesh Ewald method [36] was used to calculate the electrostatic interactions. The MD trajectories were stored at an interval of every 2 ps and then analyzed by CPPTRAJ [37] and Bio3D package [38] of R software.

2.5.1. Binding free energy calculation

Molecular mechanics Poison Boltzmann calculations, MMGBSA free energy algorithm was used to calculate the binding free energies of the protein-ligand complexes [39].

The following equation was applied to calculate the ΔG_{total}:

$$\Delta G_{total} = \Delta G_{complex} - [\Delta G_{protein} + \Delta G_{ligand}]$$

Where ΔG_{total} is the sum of the interaction energy of the gas phase in between the protein-ligand complex. On the other hand, to compute free energy per residue the following equation was applied:

$$\Delta G_{MMGBSA} = \Delta G_{vdW} + \Delta G_{ele} + \Delta G_{GB} + \Delta G_{Surf}$$

2.5.2. Residues free energy decomposition

MMGBSA free energy decomposition program of Amber21 was employed to complexes to find the core residues that were involved in the binding of protein with curcumin derivatives. Protein-ligand interaction was computed by applying the below equation.

$$\Delta G_{inhibitor\_residue} = \Delta G_{vdW} + \Delta G_{ele} + \Delta G_{ele,sol} + \Delta G_{nonpol,sol}$$

2.6. Prediction of toxicity properties of curcumin derivatives

Toxicity risks of curcumin derivatives, including mutagenic, tumorigenic, reproductive toxicity, and irritant effects were predicted using Data Warrior [40].

2.7. Prediction of ADMET and drug-likeness properties of curcumin derivatives

The increased attrition rate of the drug is associated with toxicity it may cause and poor pharmacokinetics properties [41]. The pharmacokinetics e.g TPSA, LogS, Drug-likeness, and Drug-score of curcumin derivatives were estimated by the ADMET prediction [42,43] tool, OSIRIS Property Explorer, and Qikprop (Schrodinger Suit).

2.8. Statistical analysis

The statistical package in Excel 2016 was used to calculate correlation coefficients and their significance using the regression analysis component of ANOVA.

3. Results and discussion

3.1. Molecular docking study analysis

Molecular docking is a scoring function that estimates ligand binding free energy and affinities [44]. Natural curcumin derivatives, which have been reported as a potential insecticide against *A. aegypti* [10], were docked in the active site [1] of the target, the sterol binding protein-2, HaSCP-2, to predict their binding mode affinities and binding interactions. The docked poses are shown in Fig. 1. Moreover, Table 1 shows structures, molecular weight, logP, and glide score (gscore) of docked curcumin derivatives. The glide score was in the range of −6.59 to −8.78, which is comparable to the positive control alpha-mangostin gscore of −6.51 [1] and also consistent with binding affinities of reported known inhibitors of the *A. aegypti* sterol binding protein, AeSCPI-1 [1], including cholesterol, beta-sitosterol, other sterols and fatty acids [1,45]. Furthermore, the curcumin derivatives possess drug-like properties [46] including LogP in the range of 2.47–6.1 comparable to control alpha-mangostin LogP (4.7) and molecular weights range of 364.4–530.5. Molecular docking analysis showed that curcumin derivatives have similar binding poses in the binding pocket, making predominantly hydrophobic interactions, which indicated these ligands could make strong binding interactions with key and functional active site residues in the binding pocket. The binding mode interactions are shown in Fig. 2.
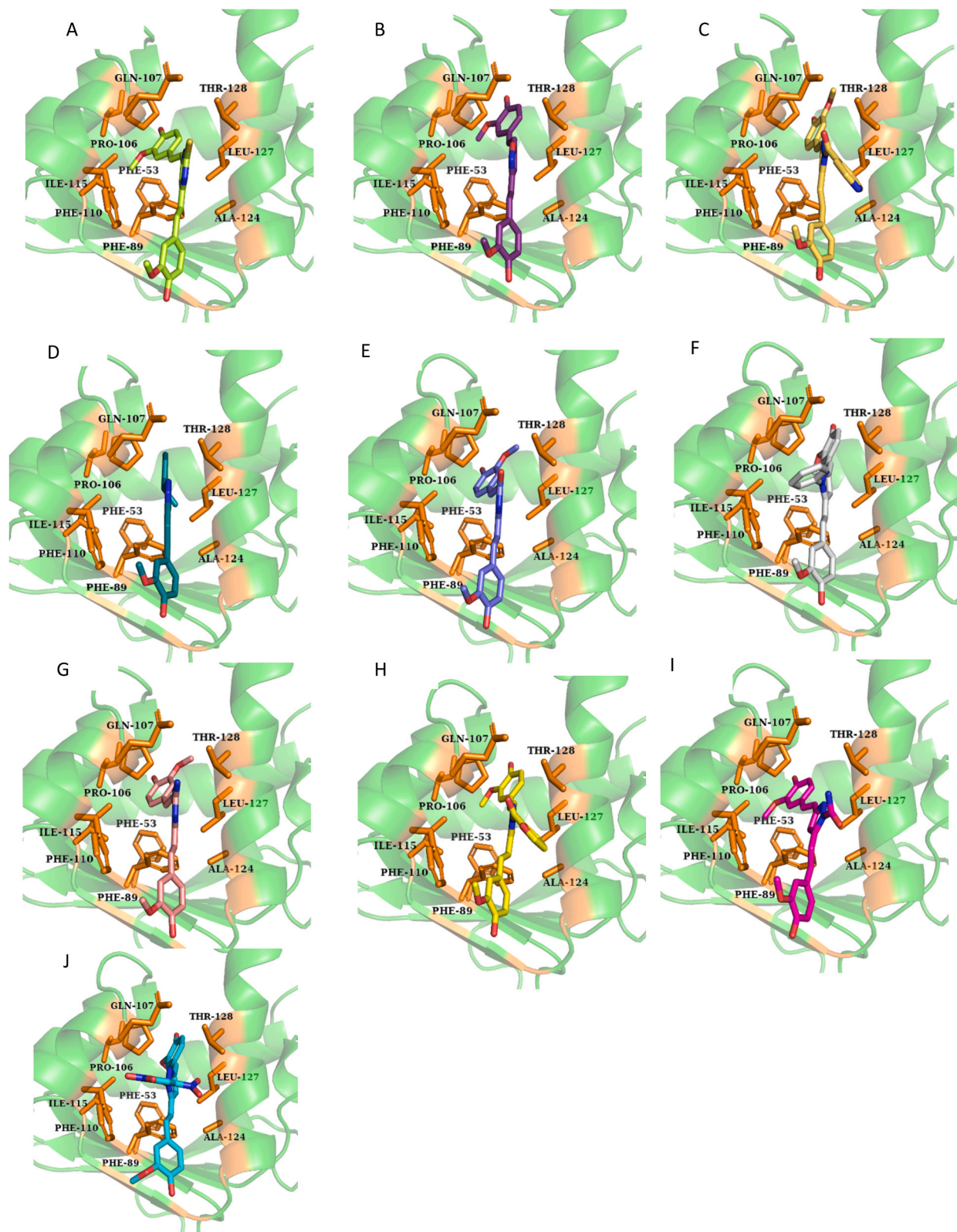
Fig. 1. Curcumin derivativesl shown docked into the binding pocket of the *Helicoverpa armigera* sterol binding protein-2, HaSCP-2. **A.** Cur01, **B.** Cur02, **C.** Cur03, **D.** Cur04, **E.** Cur05, **F.** Cur06, **G.** Cur07, **H.** Cur08, **I.** Cur09, **J.** Cur10.
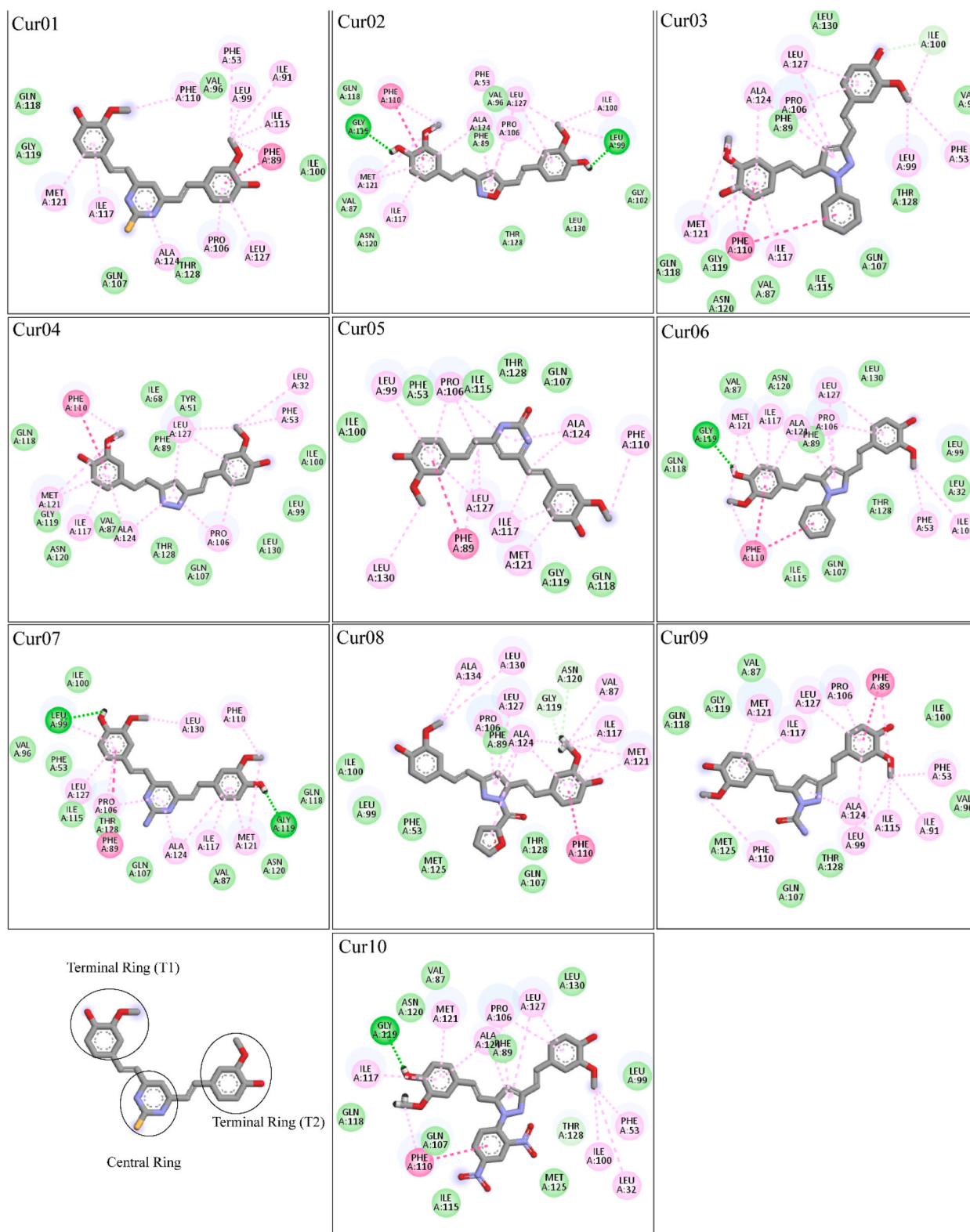
Fig. 2. Binding modes of interaction by curcumin derivatives with amino acids in the binding pocket of the *Helicoverpa armigera* sterol binding protein-2, HaSCP-2 for the indicated derivatives. Amino acid residues colored in green exhibit hydrogen bonding interactions with the bound curcumin derivatives. Magenta-colored amino acid residues exhibit pi-pi interactions with the bound curcumin derivatives. Pink-colored amino acid residues exhibit mixed pi/alkyl hydrophobic interactions with the bound curcumin derivatives.

3.1.1. Binding interaction of curcumin derivatives complexed with the target, HaSCP-2

The detailed binding interactions of curcumin derivatives with HaSCP-2 protein were predicted and modeled as shown in Fig. 2. Curcumin derivatives made mainly hydrophobic interactions with HaSCP-2 in the same fashion as cholesterol, a natural substrate does [1,2,45]. In Fig. 2, curcumin analog **Cur01** docked in the sterol binding site of HaSCP-2, has one of the methoxy groups on a terminal (T1) phenyl ring that forms Pi-alkyl hydrophobic interactions with Phe110 while making Pi-alkyl-hydrophobic interactions with Met121 and Ile117. However, **Cur01** binds in such a manner that the terminal (T2) phenyl ring forms a T-shaped Pi-Pi hydrophobic interaction with Phe89 while one of the methoxy groups attached to T2 is making alkyl-hydrophobic interaction with Ile115, Ile91, and Leu99. In the case of **Cur02** (Fig. 2), the hydroxy group on T1 makes a hydrogen bond with Gly119. However, the hydroxy group on T2 of **Cur02** makes a hydrogen bond with Leu99. Additionally, Phe110 interacts with T1 through a T-shaped Pi-Pi hydrophobic interaction, and forms alkyl-hydrophobic interactions with Met121, Ile117, and Ala124. At the same time, the central ring makes alkyl-hydrophobic interactions with Phe53 and Pro106, and the T2 aromatic ring makes alkyl-hydrophobic interactions with Pro106, Leu127, and T2 methoxy group makes alkyl-hydrophobic bonding with Ile100 and Leu127. **Cur03** (Fig. 2), interacted via a T-shaped hydrophobic Pi-Pi stacking interaction with Phe110 at T1 and with a central ring as well, while the methoxy group at T1 makes alkyl-hydrophobic interactions with Met121. Additionally, T1 is also making alkyl-hydrophobic bonding with Ile117, Ala124, and Met121. Moreover, the methoxy group at T2 is forming alkyl-hydrophobic interactions with Phe53 and Leu99. However, the central ring is interacting with Pro106, Leu127, and Ala124 by making alkyl-hydrophobic interactions. In the case of **Cur04** (Fig. 2), the main binding interactions with T1 are Pi-Pi stacked hydrophobic interactions with Phe110, and alkyl-hydrophobic interactions with Met121, Ile117, and Ala124, while T1, T2, and central ring form mixed-pi/alkyl hydrophobic interactions with Phe53, Phe110, Pro106, Leu127, Met121. With **Cur05** (Fig. 2), T1 interacts by making Pi-Pi T-shaped hydrophobic interactions with Phe89, while making alkyl-hydrophobic interactions with Leu127, Pro106, Ile117, and Ala124. However, T2 makes mixed Pi-alkyl hydrophobic interactions with Leu99, Pro106, Phe110, Leu127, Ala124, Ile117, and Met121. The hydroxy group on T1 of **Cur06** (Fig. 2) makes hydrogen bonds with Gly119, while T1 makes Pi-Pi T-shaped hydrophobic interactions with Phe110. Moreover, the methoxy group at T2 interacts by making alkyl-hydrophobic interactions with Phe53 and Ile100, while forming mixed Pi-alkyl hydrophobic interactions with Phe110, Met121, Ile117, Ala124, Pro106, and Leu127. In the case of **Cur07** (Fig. 2), the hydroxyl group on T1 forms a hydrogen bond with Leu99, while the hydroxyl group on T2 forms a hydrogen bond with Gly119. T1 is also making Pi-Pi T-shaped hydrophobic interactions with Phe89. However, one of the methoxy groups at T2 is showing alkyl-hydrophobic interactions with Phe110, and mixed Pi/alkyl hydrophobic interactions with Phe110, Met121, Ile117, Ala124, Pro106, and Leu127. **Cur08**'s (Fig. 2) T2 ring is forming Pi-Pi T-shaped hydrophobic interactions with Phe110, and alkyl-hydrophobic interactions with Met121, Ile117, Val87, and Ala124. At the same time, the central ring is making Pi-hydrophobic interactions with Pro106, Leu127, and Ala124. Also, one of the methoxy groups of T1 is interacting with Ala134 and Leu130 via making alkyl-hydrophobic interactions. In the case of **Cur09** (Fig. 2), T1 is making alkyl-hydrophobic interactions with Ile117, and Met126, and one of the methoxy groups is forming alkyl-hydrophobic interactions with Phe110. However, its T2 is making Pi-Pi T-shaped hydrophobic interactions with Phe89, and one of the methoxy groups is forming alkyl-hydrophobic with Phe53, Ile91, Ile115, Ala124, and Leu99. With **Cur10** (Fig. 2), a hydroxy group on T1 makes a hydrogen bond with Gly119 while the T1 ring makes alkyl-hydrophobic interactions with Met121 and Pro106. The central ring forms a Pi-Pi T-shaped hydrophobic interaction with Phe110, and T2 forms alkyl-hydrophobic interactions with pro106 and Leu127, while one of the methoxy groups at T2 interacts with Phe53, Ile100, and Leu32 by making alkyl-hydrophobic interactions. Thus, the molecular interactions exhibited by curcumin derivatives were predominantly hydrophobic interactions at the core with binding site residues, particularly the phenylalanine aromatic ring [1]. Our results are consistent with the observations of Ma et al. [1], that Phe53 is crucial for the binding of ligand molecules with HaSCP-2 as compared to other binding site residues. In our study, key residue Phe53 is making strong hydrophobic interactions in curcumin ligands, which was also reported for SlSCP-2 (*Spodoptera litura* sterol carrier protein-2) and AeSCP-2(*Aedes aegypti* sterol carrier protein-2) where Phe53 is equivalent to Phe32 and Tyr51 is equivalent to Tyr37, respectively [45,47]. It is suggested that the binding of curcumin derivatives with core residue phenylalanine(53, 89, 110) can impede the function of the hydrophobic cavity of HaSCP-2 because a mutation in these residues has resulted in a reduction in hydrophobic characteristics of HaSCP-2 resulting in reduced uptake or transport of cholesterol and fatty acids [1]. Based on these interaction sites, it is concluded that these active site residues in HaSCP-2 can serve as a potential insecticidal target to control the infestation of *H. armigera* by limiting the uptake of dietary sterols.

3.2. Analysis of fluorescence binding and displacement assay

Different types of binding and displacement assays have been used to characterize the binding affinity of a ligand to its receptor protein, including in the case of sterol binding proteins, the binding of NBD cholesterol fluorescent analog [1,19] or radiolabeled cholesterol [48]. These assays determine the ability of test substances like curcumins to inhibit binding to the target protein in a competitive binding manner, by competing for the binding to the hydrophobic binding site by a fluorescent probe such as 1,8-ANS, which becomes fluorescent when bound to hydrophobic proteins [45,49]. Binding affinities of curcumin derivatives with HaSCP-2 were determined using 1,8-ANS fluorescence binding and displacement from purified recombinant HaSCP-2 and compared with the positive control alpha-mangostin [1]. Reduced fluorescence emission signals were observed with increasing concentrations of curcumin derivatives(Fig. 3), showing that curcumin derivatives have a sufficiently strong binding affinity for HaSCP-2 to be able to block cholesterol and beta-sitosterol uptake and transport function of HaSCP-2 in *H. armigera* at a cellular level. The IC_{50} values of curcumin derivatives were found to be in the range of 9.64 μM–33.97 μM (Table 2), which are comparable to the IC_{50} values reported for natural compounds, including cholesterol (50.13 μM), arachidonate (18.12 μM), palmitic acid (59.05 μM), stearic acid (39.82 μM), and oleic acid (24.37 μM) [45]. Among tested curcumin compounds, **Cur10** showed the strongest binding with an IC_{50} value of 9.64

μM (Fig. 3, Table 2), while **Cur07** showed an IC$_{50}$ of 19.86 μM (Fig. 3, Table 2), and **Cur06** IC$_{50}$ was found to be 20.79 μM (Fig. 3, Table 2), which were comparable to the observed IC$_{50}$ value of control alpha-mangostin (11.46 μM) (Fig. 3, Table 2). These results also indicate that curcumin derivatives bind to HaSCP-2 and displace the 1,8-ANS probe in the same concentration-dependent manner as the positive control, alpha-mangostin. Additional curcumin analog IC$_{50}$ values are presented in Table 2.

3.3. Inhibition of insect cell line Sf9 growth in culture

Cultured cell lines have been used to study insecticide activity, including *Sf*9 cell lines [24,25], *Aedes aegypti* cell line, Aag-2, and *Manducs sexta* cell line (GV1) [50]. We used the *Sf*9 cell line to perform a cytotoxicity assay of curcumin derivatives to evaluate their inhibitory action in Sf9 cells. MTT assay was performed to calculate the percentage of cell growth inhibition rate (%IR) in *Sf*9 cells. Cell growth inhibition rates were measured by treating cells with varying concentrations (0.5 μM–100 μM) of curcumin derivatives including control alpha-mangostin. These derivatives induced cytotoxic cell death among cells of *Sf*9 in a dose-dependent manner (Fig. 4). Strikingly, cytotoxicity is more pronounced among cells treated with curcumin d derivatives than in control cells treated with alpha-mangostin (Fig. 4). In the case of a control group, alive cells with purple formazan formation were seen and the rate of cell growth inhibition rate was also found to be less in the control group than in the treated group. In the control group, the maximum inhibition rate (%IR) was recorded to be 52.18 ± 8.81 % (Fig. 4, Table 2) at 100 μM concentration. On the other hand, **Cur10** caused a maximum IR of 91.65 ± 6.51 % among cells of *Sf*9 (Fig. 4, Table 2) while the maximum IR of **Cur07** was 89.98 ± 8.16 % (Fig. 4, Table 2). The third most inhibition in cell growth rate was recorded by **Cur06**, whose %IR was 87.43 ± 10.07 % (Fig. 4, Table 2) and found to be maximum at 100 μM which corresponds to their IC$_{50}$ values, respectively. It shows that our hit compounds **Cur10**, **Cur07,** and **Cur06** can prove to be promising inhibitors of HaSCP-2 to stop the uptake of cholesterol. Surprisingly, the rest of all curcumin derivatives also showed a significant cell growth inhibition rate (Fig. 4). In the figure below we showed the %IR graphs of all curcumin derivatives which caused at least more than 50 % inhibition rate among SF9 cells during the MTT assay. Our cell-based assay result is consistent with the toxic effects of neuro-insecticides on *Sf*9 cells by Saleh et al. [24]. Moreover, cytotoxicity assays of curcumin have also been studied to evaluate their effects on *Sf*9 cells [25] where curcumin is found to cause cell death among *Sf*9 cells. It's suggested that cell growth inhibition rate (IR) was found to be maximum at 100 μM concentration of tested small curcumin derivatives after 72 h of treatment. In our study, the relative cell growth inhibition rate of each tested inhibitor molecule was surprisingly greater than control alpha-mangostin (Fig. 4 and Table 2). There was a strong, very significant negative correlation ($r(9) = -0.888$, p < .001) between inhibition of binding of curcumin derivatives to HaSCP-2, measured as 1,8-ANS displacement (IC$_{50}$ in μM), and percent inhibition of *Sf*9 cell growth at 100 μM curcumin derivatives concentration, consistent with the tested curcumin derivatives acting by binding to and inhibiting sterol uptake by HaSCP-2.

3.4. Binding mode validations through molecular dynamics simulations of selected curcumin compounds

Based on the binding affinities and plausible binding modes (Table 1, Figs. 1 and 2), inhibition effects (IC$_{50}$), and percent inhibition of *Sf*9 cell growth (% IR), a total of 3 curcumin derivatives (**Cur06**, **Cur07,** and **Cur10**) were selected to explore their stability and binding affinities with target HaSCP-2 at 100 ns. Additionally, the stability of binding by the positive control alpha-mangostin was also explored by 100 ns simulation. The curcumin derivatives yielded results comparable to simulation studies of the positive control, alpha-mangostin. The MD trajectories were analyzed by RMSD, RMSF, Rg, hydrogen bonding, MMGBSA, and residual energy contribution.

3.4.1. Root mean square deviation (RMSD) analysis of curcumin derivative complexes

The binding modes of selected curcumin derivatives were confirmed by performing RMSD. The RMSD of backbone atoms of protein was calculated to find its conformational stability with selected compounds during the simulation run [51–54]. The RMSD plot of the protein backbone of apo-protein (black) was calculated (Fig. 5A). The apo-protein attained equilibrium at around 3 ns and its RMSD
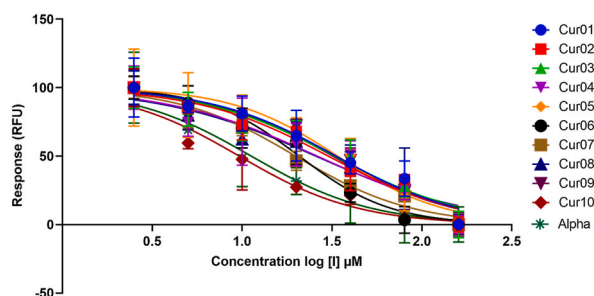

Fig. 3. Displacement Assay of 1,8-ANS in complex with HaSCP-2 by different curcumin derivatives. The displacement of probe ANS with different curcumin ligands, HaSCP-2-ANS-alpha-mangostin, HaSCP-2-ANS-Cur01, HaSCP-2-ANS-Cur02, HaSCP-2-ANS-Cur03, HaSCP-2-ANS-Cur04, HaSCP-2-ANS-Cur05, HaSCP-2-ANS-Cur06, HaSCP-2-ANS-Cur07, HaSCP-2-ANS-Cur08. The loss in signal was observed with increasing concentrations of each inhibitor molecule. Excitations were measured at 360 nm while emissions were at 480 nm.

remained in the range of 1–4 Å except for small deviations, which were observed at 30–40 ns in the range of 4–6 Å [2]. After that, the apo-protein remained stable until the end of the simulation run. Fig. 5A shows the RMSD plots of all the systems studied, including the positive control alpha-mangostin. All the complexes reached equilibrium by ~3 ns. After equilibration, all complexes remained in the range of ~3.5–5 Å except for small deviations. The RMSD plot of Cur06 (green) was found to remain in the range of 1–4 Å. **Cur07** (blue) showed higher deviations in the RMSD compared to other complexes, where its value reached ~ 6 Å and then it attained stability in RMSD value until the end the of simulation trajectory. With **Cur10** (yellow), the RMSD value remained in the range of 1–4 Å with stable conformation throughout the simulation trajectory. All the complexes showed the same trend in RMSD values in comparison to the positive control, alpha-mangostin (red), whose RMSD plot remained in the range of 1–4 Å. Thus, all the complexes remained stable during their simulation runs.

3.4.2. Root mean square fluctuation (RMSF) analysis of curcumin derivative complexes

The residual fluctuations were also calculated to confirm the binding modes and to explore the structural integrity e.g. flexibility and elastic behavior of amino acid residues of protein bound to different small molecules during the simulation run [55]. The residues with higher RMSF values indicated loop regions, whereas the residues with lower fluctuations were in rigid parts, such as the amino acids that make up alpha-helices and beta-sheets of protein. Fig. 5B shows the residual fluctuation plots of protein complexes during the 100 ns simulation. It can be observed that the start and end residues showed the highest RMSF values as these are N and C-ter-minals. All the complexes showed the same trend in RMSF analysis except for small fluctuations observed in the residues ranging from 40 to 50, 55 to 60, and 65 to 70, while other residues remained rigid during the simulation. It is suggested that overall protein structural integrity remained stable during the whole run of simulation when bound to each of the curcumin derivatives examined. The RMSF behavior of all the curcumin derivatives, when bound to HaSCP-2, was found to be comparable to the positive control alpha-mangostin (Fig. 5B). Furthermore, the overall behavioral trend of selected curcumin derivatives complexes was observed by extracting different snapshots of complexes at 0, 10, 20, 30, 40, 50, 60, 70, 80, 90, and 100 ns during the simulation trajectory and was superimposed to evaluate the position of docked derivatives, it revealed that all curcumin derivatives remained tightly bound to the active site of the target protein, HaSCP-2 (Fig. 5C).

3.4.3. Radius of gyration (Rg) analysis of curcumin derivatives

The compactness of the protein structure of complexes was evaluated by the Radius of gyration analysis [56]. The higher Rg value shows the unfolding events in the protein structure during the simulation run while the lower or stable Rg values show the compactness of the protein. Fig. 6 shows the Rg plots of curcumin derivative complexes including apo-protein (HaSCP-2). It can be observed that **Cur06** had Rg values of ~31.5 Å to 20 ns comparable to apo-protein Rg value of 31.8 Å. However, during the 20–80 ns, it showed a minor deviation of 1 Å but after 80 ns, it attained stability. The Rg values of **Cur07** (Fig. 6) showed an increase near 20 ns but attained the previous stable range at 25 ns and remained in this range till 50 ns. This complex showed deviations in the second half of simulation time, but the deviations were minor with values reaching 31.8 Å from 31.4 Å. Lastly, the Rg values of **Cur10** (Fig. 6) did not show any deviation and it remained in the range of 31.6–31.7 Å throughout the simulation trajectory. The overall Rg values of all the complexes showed that the protein remained compact comparable to the apo-protein Rg value and no protein unfolding events were observed during the simulation. Although a minor increase was observed in Rg values, it was negligible.

3.4.4. Hydrogen bonding analysis of curcumin derivatives

In this study, the H-bonding of curcumin derivatives with HaSCP-2 protein was analyzed (Fig. 6). **Cur06** (Fig. 7), formed 1 H-bond between a molecule and target HaSCP-2 during the time frame of 100 ns. **Cur07** (Fig. 7) formed nearly 2 H-bonds in the simulation trajectory. While **Cur10** (Fig. 7), overall made 1 H-bonds in a 100 ns time frame. Intermolecular H-bonding is a predictor of strong binding affinity between a ligand and a target protein. H-bonds can form or break during the simulation trajectory [57]. Thus, it is concluded that curcumin derivatives had an effective binding affinity with binding site residues of HaSCP-2 and interacted via consistent intermolecular H-bonds formation (Fig. 7).

Table 2
Inhibitory values (IC_{50} in μM) for curcumin derivatives in binding and displacement of the fluorescent probe, 1,8-ANS bound to HaSCP-2, and percent inhibition of cell growth rate (%IR) at 100 μM.

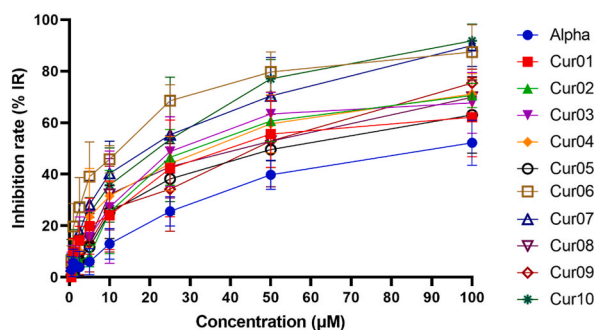| Derivative ID	IC_{50} (μM)	%IR At 100 μM
Cur01	33.31	68.14
Cur02	30.17	70.62
Cur03	32.64	67.71
Cur04	26.15	71.29
Cur05	33.97	63.02
Cur06	20.79	87.43
Cur07	19.86	89.98
Cur08	25.76	69.82
Cur09	31.96	75.39
Cur10	9.64	91.82
Alpha-mangostin (Control)	11.46	52.18

Fig. 4. Inhibition of growth of the *Sf*9 cell line in culture by curcumin derivatives. Inhibition of growth by *Sf*9 cells was measured as a reduced number of viable cells measured with an MTT assay in cultures containing the indicated concentrations of curcumin derivatives and the positive control alpha-mangostin (Alpha).

3.4.5. Analysis of binding free energy calculations

The binding free energies of **Cur06**, **Cur07**, and **Cur10** with HaSCP-2 were calculated by the MMGBSA method [58] to the last 300 frames of the MD trajectory. MMGBSA was calculated in terms of solvation energy, and gas phase energy. Table 3 shows computed binding free energy components e.g., ΔE_{vdw}, ΔE_{ele}, ΔE_{GB}, ΔE_{surf}, ΔG_{gas}, ΔG_{solv}, and the total energy of each complex, including with control alpha-mangostin. Analysis of MMGBSA revealed that the **HaSCP-2-Cur06** complex possesses high $\Delta G_{pred(GB)} = -45.51 \pm 0.45$ kcal/mol (Table 3), while the complex per frame binding free energy was in the range of -45 kcal/mol to -30 kcal/mol (Fig. 9). The **HaSCP-2-Cur07** complex showed $\Delta G_{pred(GB)} = -42.29 \pm 0.41$ kcal/mol of MMGBSA (Table 3) however, the complex per frame binding free energy was -42 kcal/mol to -30 kcal/mol (Fig. 9). These values are comparable to the MMGBSA result with the positive control, alpha-mangostin, for which the value was $\Delta G_{pred(GB)} = -42.29 \pm 0.35$ kcal/mol (Table 3). However, the results of MMGBSA of the **HaSCP-2-Cur10** complex were found to be somehow lower in comparison to the other two curcumin derivatives, namely $\Delta G_{pred(GB)} = -33.47 \pm 3.79$ kcal/mol (Table 3) and the complex per frame binding free energy was found to be -35 kcal/mol to -25 kcal/mol and showed a drop of -10 kcal/mol at around 20 ns (Fig. 9). The results of the binding free energy computation by MMGBSA were comparable to the per-frame binding free energy calculation during the simulation trajectory.

The contribution of binding site residues was computed by the energy decomposition function of MMGBSA [59]. This calculation showed that in the complex of HaSCP-2 with **Cur06**, the binding pocket residues Leu32, Phe53, Phe89, Leu99, Pro106, Phe110, Ile115, Ile117, Met121, Met125 and Leu127 made high energy contributions (Fig. 8). In the case of the complex of HaSCP-2 with **Cur07**, binding pocket residues Leu32, Phe53, Phe89, Phe110, Leu99, Pro106, Phe110, Ile115, Ile117, Met121, Met125, and Leu127 contributed greatly to the total binding free energy (Fig. 8). In the case of the complex of HaSCP-2 with **Cur10**, Phe53, Phe89, Gln107, Phe110, Ile117, Met121, and Met125 showed high contributions to the binding free energy (Fig. 8). The calculations also revealed that the key residues, Phe53, Phe89, and Phe110 contributed to the high free energy of binding in all three complexes. The residue Phe53
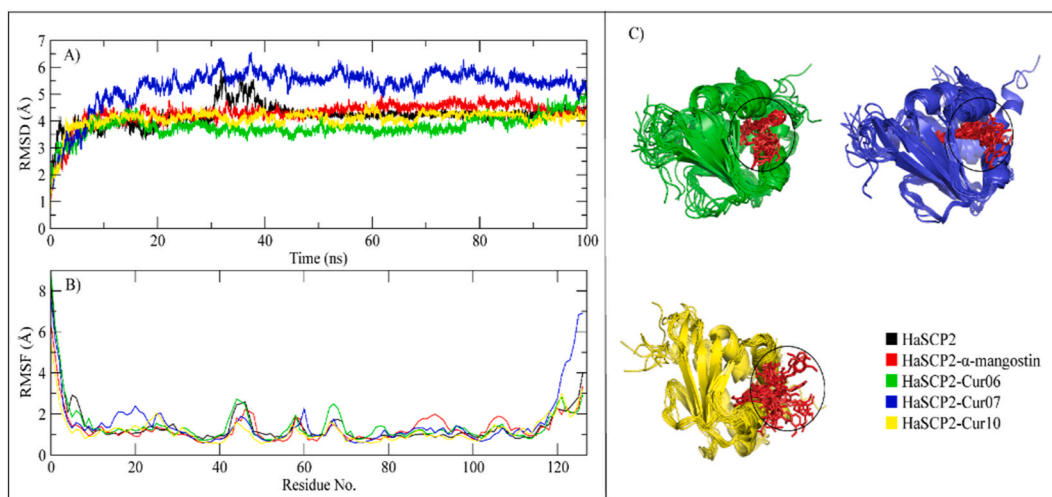

Fig. 5. A) Root mean square deviation (RMSD) plots of three selected curcumin derivatives: HaSCP-2-Cur06 complex (green), HaSCP-2-Cur07 complex (blue), and HaSCP-2-Cur10 complex (yellow), HaSCP-2 apo-protein (black), and complexed with control alpha-mangostin (red). **B)** Root mean square fluctuation (RMSF) plots of the three selected curcumin derivatives, the HaSCP-2 apo-protein, and control alpha-mangostin. **C)** Superimposed snapshots of MD trajectories of the selected curcumin derivatives with HaSCP-2-Cur06 (green), HaSCP-2-Cur07 (blue), and HaSCP-2-Cur10 (yellow).
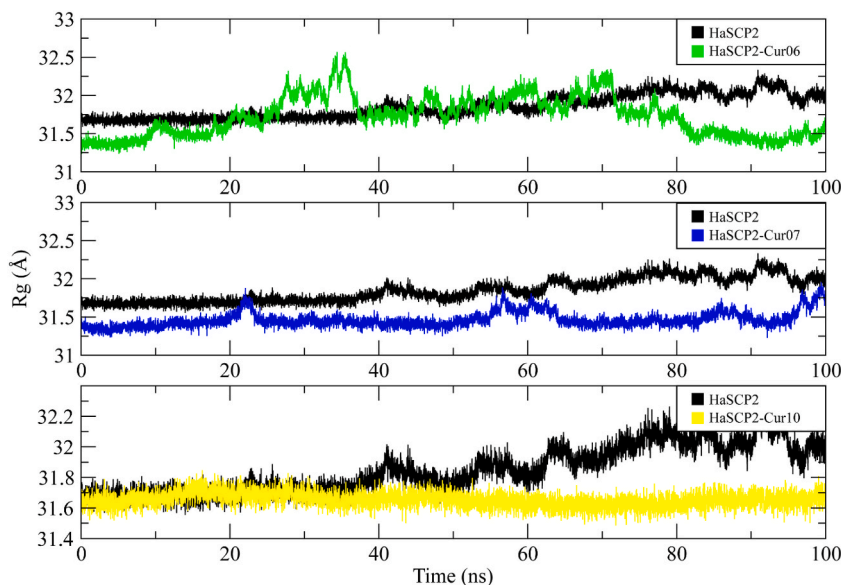
Fig. 6. The compactness of HaSCP-2 in complex with **Cur06**, **Cur07**, **Cur10**, and apo-protein (HaSCP-2) was determined by the radius of gyration analysis.
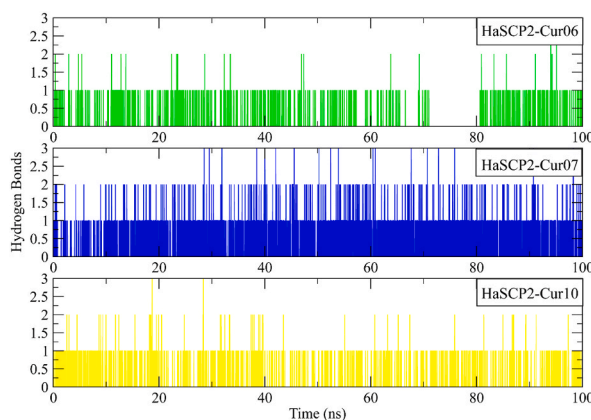

Fig. 7. Hydrogen bonding pattern of curcumin derivatives, **Cur06**, **Cur07**, and **Cur10**, a consistent hydrogen bonding trend has been observed during the time frame of 100 ns.

Table 3
Binding free energy calculations of complexes by MM/GBSA.

Complex system	HaSCP-2-alpha-mangostin	HaSCP-2-Cur06	HaSCP-2-Cur07	HaSCP-2-Cur10
$\Delta \mathbf{E_{vdw}}$	−53.32 ± 0.35	−52.28 ± 0.43	−48.04 ± 0.41	−39.53 ± 3.66
$\Delta \mathbf{E_{ele}}$	−0.96 ± 0.41	0.73 ± 0.28	−0.72 ± 0.21	−2.14 ± 2.30
$\Delta \mathbf{E_{GB}}$	18.61 ± 0.45	13.14 ± 0.28	−13.21 ± 0.22	13.21 ± 1.95
$\Delta \mathbf{E_{surf}}$	−6.61 ± 0.03	−7.19 ± 0.043	−6.75 ± 0.03	−5.02 ± 0.42
$\Delta \mathbf{G_{gas}}$	−54.29 ± 0.54	−51.55 ± 0.49	−48.76 ± 0.50	−41.67 ± 4.65
$\Delta \mathbf{G_{solv}}$	11.99 ± 0.44	6.05 ± 0.28	6.46 ± 0.21	8.19 ± 1.81
$\Delta \mathbf{G_{pred(GB)}}$	−42.29 ± 0.35	−45.51 ± 0.45	−42.29 ± 0.41	−33.47 ± 3.79

makes hydrophobic interactions that are crucial for the binding of curcumin derivatives with HaSCP-2 as compared to other binding site residues [1]. These calculations indicate how curcumin derivatives can bind to the hydrophobic cavity of HaSCP-2 and block the transport of cholesterol and other sterols, and thus have the potential to function as insecticidal agents in the control of infestation by *H. armigera* and by other insects with analogous SCP-2 proteins.
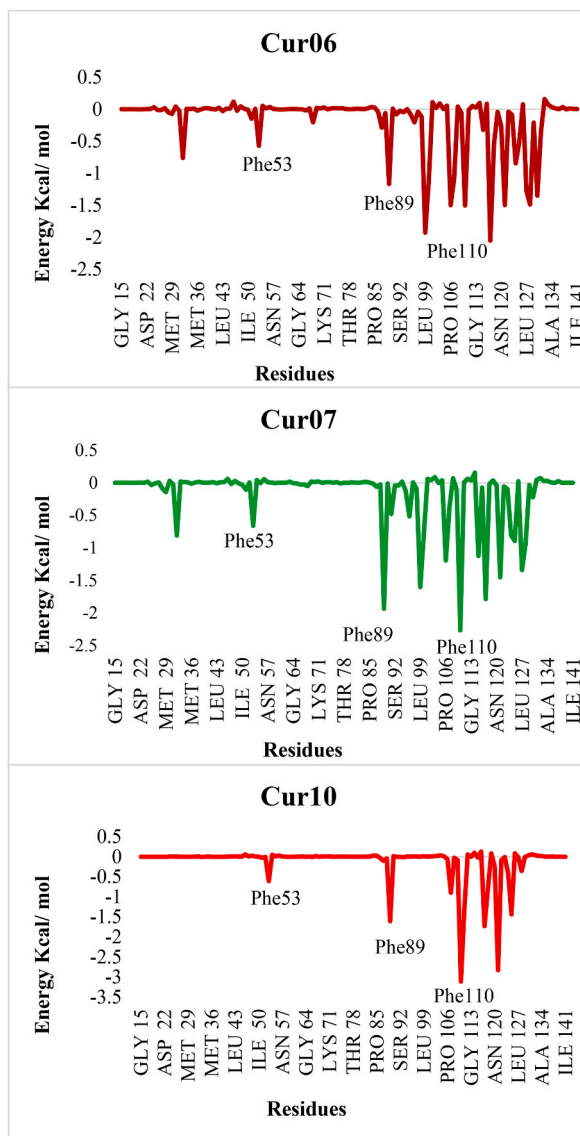
Fig. 8. Binding free energy decomposition and comparison of selected curcumin derivatives, **Cur06** (maroon), **Cur07** (green), and **Cur10** (red), and calculation of the energy contribution by three active site residues (Phe53, Phe89, Phe110) to the total binding free energy in complexes with **HaSCP-2**.

3.5. Prediction of toxicity properties of curcumin derivatives

We carried out predictions of toxicity properties of curcumin derivatives for several toxicity types, including mutagenic, tumorigenic, reproductive effective, and irritant activities using the Data Warrior tool [60]. None of the curcumin derivatives included in this study were predicted to exhibit toxic properties except **Cur03**, which was predicted to exhibit high mutagenic and reproductive toxicities, and **Cur10**, which has a low irritant level. The lack of predicted toxicity by other curcumin derivatives represents a prediction that toxicity in the curcumin derivatives can be addressed by structural modification, which is an important attribute for developing insecticides or pesticides that are effective in controlling pests while minimizing harm to non-target organisms and the environment.

3.6. Drug-likeness and ADMET analysis of lead curcumin derivatives

The predicted pharmacokinetic properties of curcumin derivatives are given in Table 4. The lead curcumin derivatives possess drug-like properties [46] including LogP in the range of 3.3–6.1 and molecular weights range of 391.4–530.5. Moreover, all the lead curcumin derivatives showed an acceptable TPSA (topological polar surface area) score. TPSA of a molecule is strongly related to its
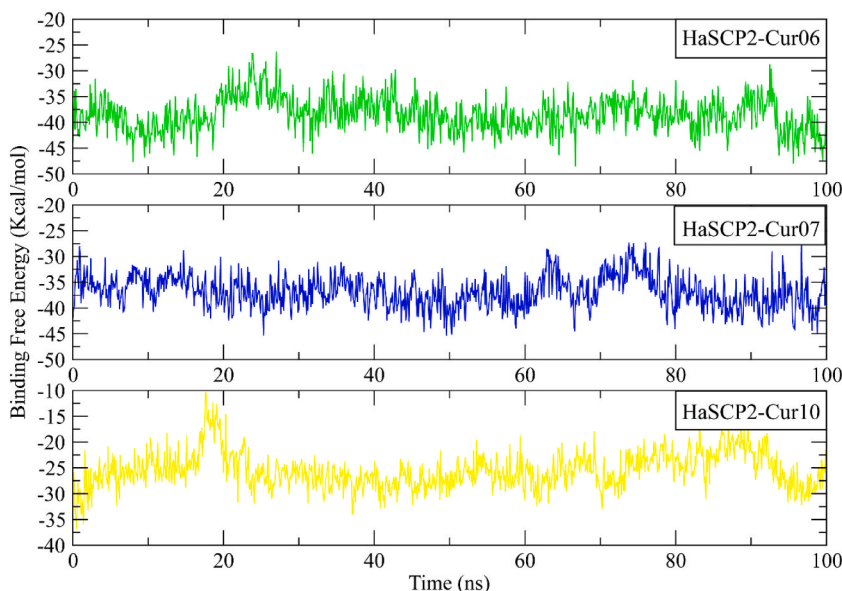
Fig. 9. Perframe binding free energy calculation of curcumin derivatives, **Cur06**, **Cur07**, **Cur10**. Per-frame binding free energy computation is comparable to the energy computation by MMGBSA.

Table 4
Predicted drug-likeness properties of lead curcumin derivatives.

Derivative ID	MW	cLogP	TPSA	LogS	Drug-likeness	Drug score
Cur06	440.5	6.1	83.55	−4.99	−8.43	0.3
Cur07	391.4	3.3	109	−3.24	0.98	0.67
Cur10	530.5	4.87	161.5	−3.28	1.73	0.34

Table 5
Predicted ADMET related properties of lead curcumin derivatives.

Derivative ID	QPlogPo/w	QPlogHERG	QPCaco2	QPlogBB	QPlogKhsa
Cur06	6.13	−7.49	872.19	−1.29	1.29
Cur07	2.33	−6.69	514.58	−2.37	0.26
Cur10	4.79	−7.17	616.59	−3.56	1.19

Recommended range: QPlogPo/w −2.0 to 6.5, QPlogHERG < −5, QPCaco2 < 25 poor; >500 great, QPlogBB −3.0 to 1.2, QPlogKhsa −1.5 to 1.5.

hydrogen bonding and is a good predictor of bioavailability [61] which reflects their good bioavailability. LogS value is concerned with solubility properties both in terms of absorption and distribution. Lead curcumin derivatives showed LogS values in an acceptable range [62]. Furthermore, the drug-likeness value of lead curcumin derivatives is in a positive range except for **Cur06** whose score is in negative value which can be addressed by making necessary structural modifications. The drug score evaluates the compound's overall potential to act as a drug. A high drug score of a compound elucidates its higher potential to be considered as a drug candidate [62]. Curcumin derivatives showed a high drug score while **Cur07** had the highest drug score of 0.67 among them. Moreover, the ADMET related properties (Table 5) of lead curcumin derivatives were also calculated. The aqueous solubility which is octanol/water partition coefficient (QPlogPo/w) values are in an acceptable range of 2.33–6.13 (Table 5) of lead curcumin derivatives. Additionally, the predicted IC_{50} value for blockage of HERG K+ channels are in the range of −6.69 to −7.49 (Table 5). On the other hand, predicted Caco-2 cell permeability (QPCaco2) falls in the range of 514.58–872.19. While the brain/blood partition coefficient (QPlogBB) and binding to human serum albumin (QPlogKhsa) values of curcumin derivatives have also shown acceptable ranges mentioned in Table 5 [63].

4. Conclusions

In conclusion, the exploration of natural compounds like curcumin derivatives as potential insecticides aligns with the growing interest in sustainable and eco-friendly pest management strategies. Chemically synthesized derivatives of curcumin showed a good

binding affinity with HaSCP-2 protein using fluorescence binding and displacement assay. Further three compounds showed good cell growth inhibition of *sf9* cells in cytotoxicity assay. MD simulation studies also revealed that these derivatives were binding well at the active site of HaSCP-2 protein through the molecular docking predicted binding modes. The predicted ADMET analysis showed that these derivatives are non-hazardous to humans and other non-target species. Therefore, we report curcumin derivatives as insecticidal agents targeting HaSCP-2 protein to block the uptake and transport of sterols to control an infestation of *H. armigera* bollworm in beneficial crops.

CRediT authorship contribution statement

Naeema Kausar: Writing – review & editing, Writing – original draft, Investigation. **Wayne Thomas Shier:** Writing – review & editing, Methodology. **Mahmood Ahmed:** Validation, Data curation. **Maryam:** Visualization, Methodology, Investigation, Visualization, Methodology, Investigation. **Norah A. Albekairi:** Visualization, Resources. **Abdulrahman Alshammari:** Writing – original draft, Visualization, Resources. **Muhammad Saleem:** Supervision, Methodology, Formal analysis. **Muhammad Imran:** Writing – original draft, Visualization, Supervision, Methodology. **Muhammad Muddassar:** Writing – review & editing, Supervision, Project administration, Funding acquisition, Conceptualization.

Declaration of competing interest

The authors declare that they have no known competing financial interests or personal relationships that could have appeared to influence the work reported in this paper.

Acknowledgement

References

[1] H. Ma, et al., NMR structure and function of Helicoverpa armigera sterol carrier protein-2, an important insecticidal target from the cotton bollworm, Sci. Rep. 5 (2015) 18186.

[2] Q. Saeed, et al., In silico and in vivo evaluation of synthesized SCP-2 inhibiting compounds on life table parameters of Helicoverpa armigera (hübner), Insects 13 (12) (2022) 1169.

[3] A.d.F. Bueno, et al., Pesticide selectivity to natural enemies: challenges and constraints for research and field recommendation, Ciência Rural. 47 (2017).

[4] B.E. Tabashnik, T. Brévault, Y. Carrière, Insect resistance to Bt crops: lessons from the first billion acres, Nat. Biotechnol. 31 (6) (2013) 510–521.

[5] X. Xu, L. Yu, Y. Wu, Disruption of a cadherin gene associated with resistance to Cry1Ac δ-endotoxin of Bacillus thuringiensis in Helicoverpa armigera, Appl. Environ. Microbiol. 71 (2) (2005) 948–954.

[6] X. Jing, S.T. Behmer, Insect sterol nutrition: physiological mechanisms, ecology, and applications, Annu. Rev. Entomol. 65 (2020) 251–271. J.A.r.o.e.

[7] A. Chaudhary, K.K. Gupta, Potentials of plant-derived sterol carrier protein inhibitors in insect management, Acta Ecol. Sin. 43 (6) (2023) 925–932.

[8] F. Yuan, et al., A systematic review and meta-analysis of randomized controlled trials on the effects of turmeric and curcuminoids on blood lipids in adults with metabolic diseases, Adv. Nutr. 10 (5) (2019) 791–802.

[9] J.A. Yáñez, et al., Intestinal lymphatic transport for drug delivery, Adv. Drug Deliv. Rev. 63 (10–11) (2011) 923–942.

[10] D.M. Anstrom, et al., Mosquitocidal properties of natural product compounds isolated from Chinese herbs and synthetic analogs of curcumin, J. Med. Entomol. 49 (2) (2012) 350–355.

[11] D. Matiadis, et al., Curcumin derivatives as potential mosquito larvicidal agents against two mosquito vectors, Culex pipiens and Aedes albopictus, Int. J. Mol. Sci. 22 (16) (2021) 8915.

[12] M.M. Attia, et al., Insecticidal effects of Curcumin (Curcuma longa) against the horse stomach bot fly, Gasterophilus intestinalis (Diptera: oestridae), Int. J. Trop. Insect Sci. 42 (1) (2022) 917–926.

[13] L. Schnarr, et al., Flavonoids as biopesticides–Systematic assessment of sources, structures, activities and environmental fate, Sci. Total Environ. (2022) 153781.

[14] M. Palma-Tenango, M. Soto-Hernández, E. Aguirre-Hernández, Flavonoids in agriculture, J.F.-f.b.t.h.h (2017) 189–201. Book.

[15] S. Stankovic, et al., Practical approaches to pest control: the use of natural compounds, in: Pests, Weeds and Diseases in Agricultural Crop and Animal Husbandry Production, IntechOpen, London, UK, 2020.

[16] E. Blitzer, I. Vyazunova, Q. Lan, Functional analysis of AeSCP-2 using gene expression knockdown in the yellow fever mosquito, Aedes aegypti, Insect Mol. Biol. 14 (3) (2005) 301–307. J.I.m.b.

[17] E.M. Zdobnov, et al., Comparative genome and proteome analysis of Anopheles gambiae and Drosophila melanogaster, Science 298 (5591) (2002) 149–159.

[18] X. Du, et al., Characterization of the sterol carrier protein-x/sterol carrier protein-2 gene in the cotton bollworm, Helicoverpa armigera, J. Insect Physiol. 58 (11) (2012) 1413–1423.

[19] M.S. Kim, Q. V.L. Wessely, Identification of mosquito sterol carrier protein-2 inhibitors, J. Lipid Res. 46 (4) (2005) 650–657.

[20] R.T. Larson, et al., The biological activity of α-mangostin, a larvicidal botanic mosquito sterol carrier protein-2 inhibitor, J. Med. Entomol. 47 (2) (2014) 249–257.

[21] V.V. Oberemok, et al., A short history of insecticides, J. Plant Protect. Res. 55 (3) (2015).

[22] M. Ahmed, et al., Azomethines, isoxazole, N-substituted pyrazoles and pyrimidine containing curcumin derivatives: urease inhibition and molecular modeling studies, Biochem. Biophys. Res. Commun. 490 (2) (2017) 434–440.

[23] J. Edqvist, et al., Plants express a lipid transfer protein with high similarity to mammalian sterol carrier protein-2, J. Biol. Chem. 279 (51) (2004) 53544–53553.

[24] M. Saleh, J. Hajjar, A. Rahmo, Effect of selected insecticides on Sf9 insect cell line, Leban. Sci. J. 14 (2) (2013) 115.

[25] S. Veeran, et al., Curcumin induces autophagic cell death in Spodoptera frugiperda cells, Pestic. Biochem. Physiol. 139 (2017) 79–86.

[26] M.D. Summers, Milestones leading to the genetic engineering of baculoviruses as expression vector systems and viral pesticides, Adv. Virus Res. 68 (2006) 3–73.

[27] J.-W. Liu, et al., Parthenolide induces proliferation inhibition and apoptosis of pancreatic cancer cells in vitro, J. Exp. Clin. Cancer Res. 29 (1) (2010) 1–7.

[28] W. Humphrey, A. Dalke, K. Schulten, VMD: visual molecular dynamics, J. Mol. Graph. 14 (1) (1996) 33–38.

[29] J.C. Phillips, et al., Scalable molecular dynamics with NAMD, J. Comput. Chem. 26 (16) (2005) 1781–1802.

[30] S.-H. Ahn, et al., Data for molecular dynamics simulations of Escherichia coli cytochrome bd oxidase with the Amber force field, Data Brief 38 (2021) 107401.

[31] D.A. Case, et al., Amber 2021, University of California, San Francisco, 2021.

[32] Z. Li, et al., Parametrization of trivalent and tetravalent metal ions for the OPC3, OPC, TIP3P-FB, and TIP4P-FB water models, J. Chem. Theor. Comput. 17 (4) (2021) 2342–2354.

[33] X. Cui, et al., Extensive evaluation of environment-specific force field for ordered and disordered proteins, Phys. Chem. Chem. Phys. 23 (21) (2021) 12127–12136.

[34] B. Seo, et al., Topology automated force-field interactions (TAFFI): a framework for developing transferable force fields, J Journal of Chemical Information and Modelling 61 (10) (2021) 5013–5027.

[35] M. Pechlaner, et al., A method to apply bond-angle constraints in molecular dynamics simulations, J. Comput. Chem. 42 (6) (2021) 418–434.

[36] S. Jin, et al., A random batch Ewald method for particle systems with Coulomb interactions, SIAM J. Sci. Comput. 43 (4) (2021) B937–B960.

[37] R. Weinzierl, Molecular dynamics simulations of human FOXO3 reveal intrinsically disordered regions spread spatially by intramolecular electrostatic repulsion, Biomolecules 11 (6) (2021) 856.

[38] B.J. Grant, L. Skjaerven, X.Q. Yao, The Bio3D packages for structural bioinformatics, Protein Sci. 30 (1) (2021) 20–30.

[39] H. Sun, et al., Assessing the performance of MM/PBSA and MM/GBSA methods. 5. Improved docking performance using high solute dielectric constant MM/GBSA and MM/PBSA rescoring, Phys. Chem. Chem. Phys. 16 (40) (2014) 22035–22045.

[40] M. de Barros, et al., Pharmacological Reports about Gastroprotective Effects of Methanolic Extract from Leaves of Solidago Chilensis (Brazilian Arnica) and its Components Quercitrin and Afzelin in Rodents, 2016, pp. 403–417.

[41] F.E. Agamah, et al., Computational/in silico methods in drug target and lead prediction, Briefings Bioinf. 21 (5) (2020) 1663–1675.

[42] E. Koç, A. Üngördü, F. Candan, Antioxidant activities of Alyssum virgatum plant and its main components, Struct. Chem. (2021) 1–13.

[43] G.O. Oduselu, et al., Homology modelling and molecular docking studies of selected substituted benzo [d] imidazole-1-yl) methyl) benzimidamide scaffolds on Plasmodium falciparum adenylosuccinate lyase receptor, Bioinf. Biol. Insights 13 (2019) 1177932219865533.

[44] J. Li, A. Fu, L. Zhang, An overview of scoring functions used for protein–ligand interactions in molecular docking, nterdisciplinary Sciences: Computational Life Sciences 11 (2019) 320–328. J.I.S.C.L.S.

[45] L. Zhang, et al., Structural and functional analyses of a sterol carrier protein in Spodoptera litura, PLoS One 9 (1) (2014) e81542.

[46] C.A. Lipinski, Lead-and drug-like compounds: the rule-of-five revolution, Drug Discov. Today Technol. 1 (4) (2004) 337–341. J.D.d.t.T.

[47] J.T. Radek, D.H. Dyer, Q. Lan, Effects of mutations in Aedes aegypti sterol carrier protein-2 on the biological function of the protein, Biochemistry 49 (35) (2010) 7532–7541.

[48] K. Krebs, Q. Lan, Isolation and expression of a sterol carrier protein-2 gene from the yellow fever mosquito, Aedes aegypti, Insect Mol. Biol. 12 (1) (2003) 51–60.

[49] C.D. Kane, D.A. Bernlohr, A simple assay for intracellular lipid-binding proteins using displacement of 1-anilinonaphthalene 8-sulfonic acid, Anal. Biochem. 233 (2) (1996) 197–204.

[50] M.-s. Kim, V. Wessely, Q. Lan, Identification of mosquito sterol carrier protein-2 inhibitors, J. Lipid Res. 46 (4) (2005) 650–657. J.J.o.l.r.

[51] N.G. Arakal, et al., Ligand-based design approach of potential Bcl-2 inhibitors for cancer chemotherapy, Comput. Methods Progr. Biomed. 209 (2021) 106347.

[52] S. Krishna, et al., Structure-based design approach of potential BCL-2 inhibitors for cancer chemotherapy, Comput. Biol. Med. 134 (2021) 104455.

[53] N. Kumar, et al., Molecular binding mechanism and pharmacology comparative analysis of noscapine for repurposing against SARS-CoV-2 protease, J. Proteome Res. 19 (11) (2020) 4678–4689.

[54] K. Sargsyan, C. Grauffel, C. Lim, How molecular size impacts RMSD applications in molecular dynamics simulations, J. Chem. Theor. Comput. 13 (4) (2017) 1518–1524.

[55] H.L. Barazorda-Ccahuana, et al., Art v 4 protein structure as a representative template for allergen profilins: homology modeling and molecular dynamics 3 (12) (2018) 17254–17260.

[56] M.Y. Lobanov, N. Bogatyreva, O. Galzitskaya, Radius of gyration as an indicator of protein structure compactness, Mol. Biol. 42 (2008) 623–628.

[57] M. Surti, et al., Ilimaquinone (marine sponge metabolite) as a novel inhibitor of SARS-CoV-2 key target proteins in comparison with suggested COVID-19 drugs: designing, docking and molecular dynamics simulation study, RSC Adv. 10 (62) (2020) 37707–37720.

[58] S. Genheden, U. Ryde, The MM/PBSA and MM/GBSA methods to estimate ligand-binding affinities, Expet Opin. Drug Discov. 10 (5) (2015) 449–461.

[59] T.A. Chohan, et al., Molecular simulation studies on the binding selectivity of 2-anilino-4-(thiazol-5-yl)-pyrimidines in complexes with CDK2 and CDK7, Mol. Biosyst. 12 (1) (2016) 145–161.

[60] M. de Barros, et al., Pharmacological reports about gastroprotective effects of methanolic extract from leaves of Solidago chilensis (Brazilian arnica) and its components quercitrin and afzelin in rodents, N. Schmied. Arch. Pharmacol. 389 (2016) 403–417.

[61] P. Gogoi, et al., In silico study, synthesis, and evaluation of the antimalarial activity of hybrid dimethoxy pyrazole 1, 3, 5-triazine derivatives, J. Biochem. Mol. Toxicol. 35 (3) (2021) e22682.

[62] S. Behrouz, et al., Design, synthesis, and in silico studies of novel eugenyloxy propanol azole derivatives having potent antinociceptive activity and evaluation of their β-adrenoceptor blocking property, Mol. Divers. 23 (2019) 147–164.

[63] A. Kumar, et al., Identification of new SUMO activating enzyme 1 inhibitors using virtual screening and scaffold hopping, Bioorg. Med. Chem. Lett 26 (4) (2016) 1218–1223.